Fearon, Olesya; Kuitunen, Susanna; Ruuttunen, Kyösti; Alopaeus, Ville; Vuorinen, Tapani

Detailed Modeling of Kraft Pulping Chemistry. Delignification

Published in:
Industrial and Engineering Chemistry Research

DOI:
10.1021/acs.iecr.0c02110

Published: 22/07/2020

Document Version
Publisher's PDF, also known as Version of record

Please cite the original version:
Fearon, O., Kuitunen, S., Ruuttunen, K., Alopaeus, V., & Vuorinen, T. (2020). Detailed Modeling of Kraft Pulping Chemistry. Delignification. *Industrial and Engineering Chemistry Research*, *59*(29), 12977-12985.
https://doi.org/10.1021/acs.iecr.0c02110

I&EC research
Industrial & Engineering Chemistry Research

pubs.acs.org/IECR Article

Detailed Modeling of Kraft Pulping Chemistry. Delignification

Olesya Fearon,* Susanna Kuitunen, Kyösti Ruuttunen, Ville Alopaeus, and Tapani Vuorinen

Cite This: *Ind. Eng. Chem. Res.* 2020, 59, 12977−12985

Read Online

ACCESS | Metrics & More | Article Recommendations

ABSTRACT: This work introduces a phenomena-based model for delignification in the kraft pulping process. The solubilization of lignin is described as a set of chemical reactions representing the entire chemistry of lignin degradation as well as dissolution of the degraded lignin. For modeling, reaction mechanisms and reactions kinetics derived mainly from the literature were used. Each reaction was simulated separately and then combined for the overall degradation. The model was validated with experimental results from pine wood meal pulping under a wide range of reaction parameters. The experimental data presented a good fit with the model. With the aid of the model, the structure and the amount of wood components, in fibers and black liquor, can be determined at any pulping stage. Several engineering parameters can be computed from the detailed chemical composition of liquor and wood or chemical pulp. These include, e.g., kappa number, brightness, yield, active alkali, effective alkali, sulfidity, and higher heating value.

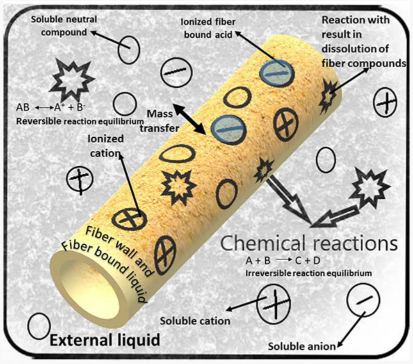

■ INTRODUCTION

The kraft pulping process introduced in 1879[1] is still the dominant method of producing chemical pulps. The purpose of any chemical pulping process is to facilitate the separation of the individual fibers in the feedstock by the dissolution of lignin.[2] In addition to purely chemical events, these processes comprise a number of morphological and physical phenomena.[3,4] Nowadays, novel approaches in biorefining, which refers to sustainable processing of biomass into a spectrum of biobased products,[5] open new opportunities to improve the current production methods. The traditional pulping industry has already adopted broader biorefinery concepts,[6] for coproduction of biofuels, biogas, and other new products. Additionally, conversion of lignin into such products as chelating agents, antioxidants, pesticides, vanillin, phenols, fertilizers, adhesives, and formaldehyde-free phenolic resin is of high interest in various industries.[7−9]

Computational simulation models are excellent and cheap supporting tools for process development, and several of them have been devised to optimize the pulping process. The first study of kraft pulping kinetics was presented by Vroom.[10] He implemented the concept "*H*-factor" that combines the pulping temperature and time as a single variable. The idea is that all pulping processes characterized by the same numerical *H*-factor value for time and temperature produce pulp of equivalent residual lignin content. Later, Hatton[11] implemented a model that predicts the kappa number and yield, based on the *H*-factor and effective alkali (EF) charge. This model is applicable to pulping of thin chips of a variety of wood species. The main disadvantages of Hatton's model is that it does not take into account the effects of varying sulfidity and liquor-to-wood ratio (L:W).[12] Additionally, Hatton's model does not predict hardwood pulping as well as it does softwood pulping.[11] Vroom's and Hatton's models are currently widely used globally in the pulping industry. Kerr[4] implemented a model where the kappa number is predicted as a function of the *H*-factor. Smith's kinetic model[13] is the most complex one and divides wood material into five components: high-reactivity lignin, low-reactivity lignin, cellulose, galactoglucomannan, and arabinoxylan. Also, many other models have been created; for example, models by Kleinert,[14] Saltin,[15] Burazin and McDonough,[16] as well as Gustafson[17] and LeMon and Teder[18] divide the delignification process into three phases (initial, bulk, residual) that are described by their own delignification rate equations. Smith and Williams[13] divided lignin into fast and slowly reacting parts in their modeling approach. In their model, the more reactive lignin was thought to possess β-ether bonds while the less reactive lignin was described to contain γ-ether bonds. Nieminen[19] developed a lignin degradation model based on a simplified Purdue model, containing two lignin subcomponents with different reactivities. Bogren[20] presented a general kraft delignification model, based on continuous distribution of reactivity types; however, the model is limited to softwood and its ability to predict industrial-like pulping processes is not satisfactory. Choi's

Received: April 26, 2020
Revised: June 24, 2020
Accepted: June 24, 2020
Published: June 24, 2020

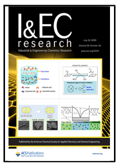

https://dx.doi.org/10.1021/acs.iecr.0c02110

Table 1. Lignin Substructures Included in the Pulping Model

structure	abbrev	explanation	figure
S1	nphG	non-phenolic (etherified) guaiacyl	Figure 1b
S2	αCOnphG	non-phenolic guaiacyl with α-carbonyl group	Figure 1c
S3	G	guaiacyl phenol	Figure 1a
S4	G$^-$	guaiacyl phenolate (ionized)	Figure 1a
S5	αβconjG	guaiacyl phenol with conjugated carbon−carbon double bond	Figure 1a
S6	αβconjG$^-$	guaiacyl phenolate with conjugated carbon−carbon double bond (ionized)	like **S5**, but OH$_{phen}$ not dissociated
S7	αCOG$^-$	guaiacyl phenolate with α-carbonyl group	Figure 1c
S8	GγβS$^-$	guaiacyl phenolate with α,β-thiirane structure	Figure 1a
S9	αCOnphGβγconj	non-phenolic guaiacyl with α-carbonyl group and conjugated carbon−carbon double bond	Figure 1c
S10	αCOnphGβγS	non-phenolic guaiacyl with α-carbonyl group and β,γ-thiirane structure	Figure 1c
S11	nphGαβO	non-phenolic guaiacyl with α,β-oxirane structure	Figure 1b
S12	nphGβNu	non-phenolic guaiacyl with attached nucleophile to β carbon in propane side chain	Figure 1b
S13	Cat	catechol	Figure 1d
S14	GαβO$^-$	guaiacyl phenolate with α,β-oxirane structure	Figure 1a
S15	nphGdem	demethylated non-phenolic guaiacyl	Figure 1d

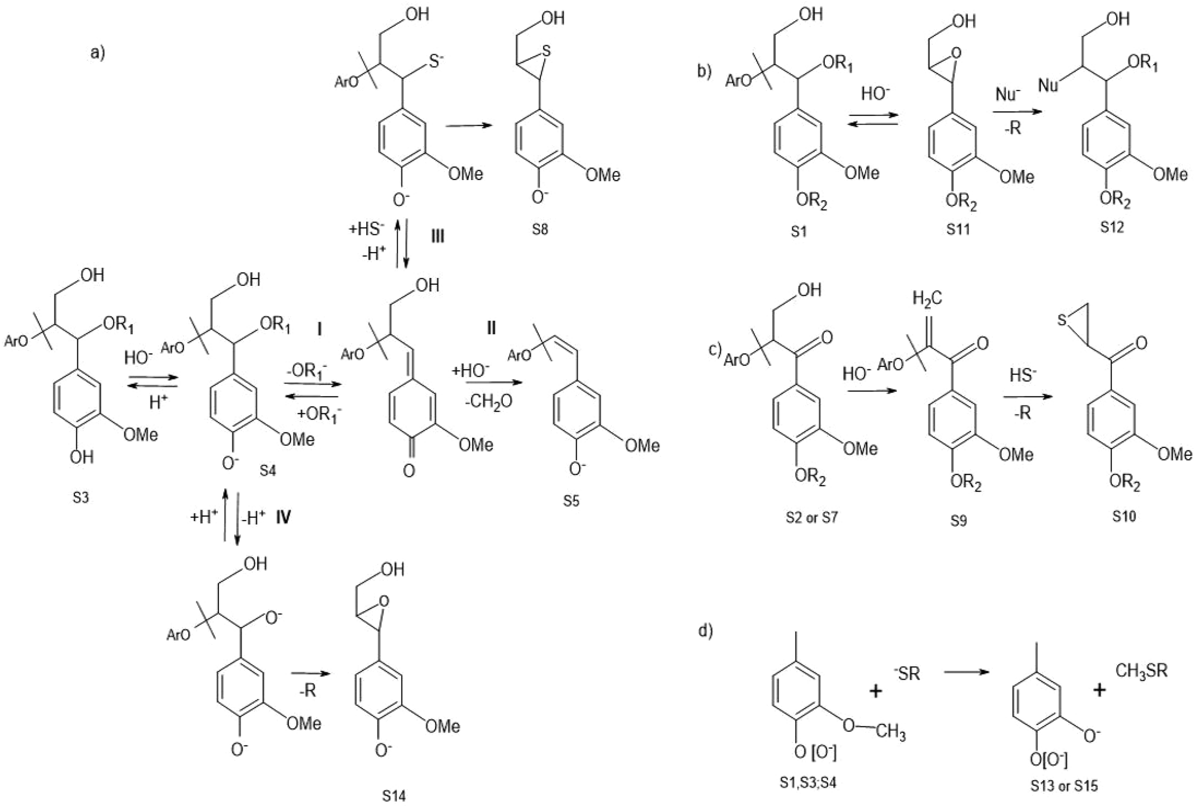

Figure 1. Lignin reactions included in the kraft pulping model. R, R_1, and R_2 denote alkyl or aryl groups or a proton.

work[21,22] presented a multiscale modeling system for the delignification process of hardwood chips. His model was able to regulate the kappa number and porosity to desired values. All models mentioned above have shown adequate prediction results; nonetheless many of them are limited by the type of wood (softwood or hardwood). Moreover, the mentioned models do not provide insight into the reaction mechanisms.

In the current work, we aimed to create a model where the real chemistry and other essential phenomena, taking place in kraft pulping, are implemented in the model at the molecular level. This approach means that the various reactions taking place in kraft pulping need to be included in the model in a comprehensive and accurate way, different from the previous kraft pulping models. With the model, it is possible to determine the structure of the wood components in the fiber and black liquor at any stage of the pulping process. The simulator should work as a tool to help in understanding the kraft pulping process in more detail.

■ MODEL

Basic Principles. The overall idea of this work was to use the kinetic parameters from lignin model compound studies and apply them for developing a simulation model. Additional hypothesis was done on how to model lignin dissolution.

The main modeling principle was to consider reactions and mass transfer phenomena of true chemical components (water, hydroxide ion, hydrogen sulfide ion, sodium ion, methyl mercaptan, methanol, etc.) and pseudocomponents in the cases where using true chemical components was not possible. In order to account for the Donnan effect, a two liquid phase approach was used. The wood fiber constituents were assumed to be present in the fiber-bound liquid. The initial amount of water bound to the fiber wall was set according to the fiber saturation point (FSP) determined to be 0.35 kg of water (kg of oven-dried wood)$^{-1}$.[23,24] More detailed descriptions of the Donnan effect and mass transfer modeling can be found in previous publications.[25,26] The modeling of changes in the FSP, caused by the degradation and dissolution of the cell wall polymers, is described in Kuitunen's work.[25]

Considering the complexity of lignin structure, it was simplified in the model where each lignin pseudocompound represents a group of real components with related structures and chemical properties. The full range of lignin structures used in the model is presented in Table 1 and Figure 1. The macromolecular aspect of lignin was considered in modeling lignin dissolution.

The monomeric lignin pseudounits were assumed to be linked to each other through β-*O*-4 linkages, which are the dominant type of linkages in lignin. Phenolic and non-phenolic lignin units react at different rates. Thus, phenolic and non-phenolic units were treated separately in the model. The main fragmentation reactions of lignin in alkaline media are the cleavage of β-aryl ether bonds.[1] The amount of β-aryl ether bonds is about 45−50% in softwood lignin and 60% in hardwood lignin.[27] This reaction leads not only to lignin fragmentation, but also to the simultaneous liberation of a new phenolic hydroxyl group. Cleavage of β-ether bonds therefore promotes lignin solubility in two ways: decreasing the molecular weight and increasing the phenolic hydroxyl group content. Lignin dissolution was modeled as a transfer process of molecules from the insoluble fiber wall to the fiber-bound liquid.[28,29] In the current model, lignin−carbohydrate bonds and lignin condensation reactions were not taken in consideration. The wood composition was estimated using the literature on a similar type of wood[1] and from the experimental results[30−32] (Table 2).

In the current work, properties of Scots pine were used for model development and validation. However, it is assumed that the model should be as applicable for softwood as it is for hardwood pulping simulation. The model idea is that wood components and their content entered depending on the wood source and type. Consequently, a difference in hardwood and softwood could be reflected in the model by introduced data on wood composition. The initial composition of chemical liquor varied depending on the experimental setup. The reaction conditions such as temperature, pressure, and consistency were obtained or calculated according to the experiments. Extremely fast mass transfer was assumed; this is the reason why wood meal studies were used for model validation and parameter optimization. The model of mass transfer in wood chips was developed; however, it is not published yet. Computer regression with Kinfit software[33] was first utilized to obtain the unknown reaction rate parameters.

Lignin Fragmentation Reactions. The list of all lignin reactions included in the model is presented in Table 3. All lignin fragmentation reactions were assumed to proceed similarly in the fiber wall and in the liquor, so the same kinetic parameters and reaction routes apply to lignin pseudocompounds in the liquid phase (dissolved) and in the fiber wall. The stoichiometry and kinetics of the lignin fragmentation reactions were based on the lignin model compound studies. The Arrhenius parameters were applied from the literature (frequency factor was calculated based on published activation energies and reaction rates) or regressed against experimental data in the present study. The confidence limit was 93−97% in the regressed values.

Table 2. Composition of Scots Pine (*Pinus sylvestris* L.) Used for Simulations[1,30−32]

component	content %	content mol/kg
lignin	26.8	
non-phenolic (etherified) guaiacyl		1.07
guaiacyl phenol		0.32
non-phenolic guaiacyl with carbonyl group in α carbon		0.0081
cellulose	41.8	
group in middle of the cellulose chain		2.466535
reducing end group of cellulose chain		0.000245
nonreducing end group of cellulose chain		0.000223
glucomannnan	16.9	
glucomannan group in middle of the chain		1.02
reducing end group in glucomannan		0.0102
nonreducing end group in glucomannan		0.0102
arabinoxylan	8.4	
group in the middle of the xylan chain		0.5784
reducing end group of xylan chain		0.0056
nonreducing end group of xylan chain		0.0056
4-*O*-methyl-D-glucuronic acid		0.08
other carbohydrates	1.5	
arabinogalactan galactose nonreducing end group		0.0106
arabinogalactan middle group		0.0160
arabinogalactan arabinose nonreducing end group		0.0071
methyl esterified galacturonan middle group		0.2308
galacturonan middle group (nonesterified)		0.1539
arabinose structure in hemicellulose		0.00056
extractives	3.4	
Ca		0.00021
K		0.00029
Mg		0.00007

Reactions of Phenolic Lignin Units. The reaction of phenolic β-*O*-4 structures **S3** (G) (Figure 1, reaction a) begins with the reversible formation of an unstable quinone methide (QM).[3] The quinone methide may undergo several reactions depending on the alkaline environment. In the absence of hydrogen sulfide, the degradation of QM proceeds mainly via elimination of formaldehyde, and as a result, the enol ether **S5** ($\alpha\beta$conjG) is formed (Figure 1, reaction a). Activation energy for the phenolic lignin degradation in alkaline conditions, with formation of the $\alpha\beta$conjG structure, has been reported by Gierer[34] and Kondo.[35] For precise values, kinetic parameters were fitted with Kinfit software and the obtained values (Table 3, reaction 2) were utilized in the model. In the presence of hydrogen sulfide, the formation of QM is followed by a nucleophilic attack of hydrogen sulfide ion which leads to subsequent fragmentation through an intramolecular S_N2 reaction (Figure 1, reaction a) yielding the thiirane structure **S7** (G$\gamma\beta$S$^-$). Gierer,[3,34] Kondo,[35] and Miksche[36] have reported activation energy values for this reaction. It is known that other competing reactions also take place: in the presence of nucleophiles from lignin or carbohydrates, condensation products may be formed.[37−39] However, this was not included in the model. Alkali-promoted

Table 3. Reaction Library and Kinetic Parameters Implemented in the Model

R	reaction stoichiometry	rate equation (k^*)	k(25 °C), s^{-1}	A, s^{-1}	E_a, kJ mol^{-1}
1	$G^- + HS^- + \mathrm{nphG} \rightarrow G\gamma\beta S^- + G$	$[G^-][HS^-]$	3.74×10^{-9}	1.3×10^{13}	120.1 ± 4.2[34]
2	$G^- + OH^- \rightarrow \alpha\beta\mathrm{conj}G^- + \mathrm{formaldehyde} + OH^-$	$[G^-][OH^-]$	4.91×10^{-10}	4.8×10^{13}	128.3 ± 7.6[35]
3	$G^- + \mathrm{nphG} + OH^- \rightarrow G\alpha\beta O^- + G^-$	$[G^-][OH^-]$	6.82×10^{-5}	1.4×10^{10}	122.7 ± 3.4[35]
4	$\alpha\mathrm{COnphG} + OH^- \rightarrow \alpha\mathrm{COnphG}\beta\gamma\mathrm{conj} + OH^- + H_2O$	$[\alpha\mathrm{COnphG}][OH^-]$	6.24×10^{-3}	3.9×10^{8}	69.1 ± 4.3[42]
5	$\alpha\mathrm{COnphG}\beta\gamma\mathrm{conj} + \mathrm{nphG} + HS^- \rightarrow \alpha\mathrm{COnphG}\beta\gamma S + G^-$	$[\alpha\mathrm{COnphG}\beta\gamma\mathrm{conj}][HS^-]$	5.29×10^{-1}	2.7×10^{3}	42.4 ± 0.9[42]
6	$2\mathrm{nphG} + OH^- \rightarrow \mathrm{nphG}\alpha\beta O + G^-$	$[\mathrm{nphG}][OH^-]$	6.73×10^{-11}	2.4×10^{11}	123.4 ± 5.1[3]
7	$\mathrm{nphG} + HS^- \rightarrow \mathrm{nphGdem}^- + \mathrm{MetMer}$	$[\mathrm{nphG}][HS^-]$	4.75×10^{-12}	1.5×10^{6}	86.5 ± 7.3[46]
8	$\mathrm{nphG} + \mathrm{MetMer}^- \rightarrow \mathrm{DiMetS} + \mathrm{nphGdem}^-$	$[\mathrm{nphG}][\mathrm{MetMer}^-]$	5.71×10^{-10}	1.8×10^{5}	75.7 ± 5.9[a]
9	$G + HS^- \rightarrow \mathrm{MetMer} + \mathrm{Cat}^-$	$[G][HS^-]$	4.75×10^{-12}	1.5×10^{6}	86.5 ± 7.3[a]
10	$G + \mathrm{MetMer}^- \rightarrow \mathrm{Cat}^- + \mathrm{DiMetS}$	$[G][\mathrm{MetMer}^-]$	5.71×10^{-10}	1.8×10^{5}	75.7 ± 5.9[a]
11	$2\mathrm{MetMer} \rightarrow \mathrm{DiMetS} + HS^- + H^+$	$[\mathrm{MetMer}]^2$	1.6×10^{-10}	5.3×10^{5}	86.5 ± 7.3[a]
		Lignin Dissolution			
12	$\mathrm{nphG}\alpha\beta O(f) + 1.7G(-f) \rightarrow \mathrm{nphG}\alpha\beta O(aq) + 1.7G(-aq)$	$[\mathrm{nphG}\alpha\beta O][G^-]$	1.29×10^{4}	8.0×10^{5}	10[b]
13	$\mathrm{nphG}\alpha\beta O(f) + 1.7\alpha\beta\mathrm{conj}G(-f) \rightarrow \mathrm{nphG}\alpha\beta O(aq) + 1.7\alpha\beta\mathrm{conj}G(-aq)$	$[\mathrm{nphG}\alpha\beta O][\alpha\beta\mathrm{conj}G\ ^-]$	3.32	1.0×10^{5}	25[b]
14	$G\gamma\beta S^-(f) + 1.5G^-(f) \rightarrow G\gamma\beta S^-(aq) + 1.5G^-(aq)$ $G\gamma\beta S^-(f) + 1.5\ G^-(f) \rightarrow G\gamma\beta S^-(aq) + 1.5\ G(aq)$	$[G\gamma\beta S^-][G]$	1.29×10^{4}	8.0×10^{5}	10[b]
15	$\mathrm{nphG}\alpha\beta O(f) + 1\mathrm{Cat}(-f) \rightarrow \mathrm{nphG}\alpha\beta O(aq) + 1\mathrm{Cat}(-aq)$	$[\mathrm{nphG}\alpha\beta O][\mathrm{Cat}^-]$	4.98×10^{3}	1.5×10^{8}	25[b]
16	$\mathrm{nphG}\alpha\beta O(f) + 0.7\mathrm{nphGdem}(-f) \rightarrow \mathrm{nphG}\alpha\beta O(aq) + 0.7\mathrm{nphGdem}(-aq)$	$[\mathrm{nphG}\alpha\beta O][\mathrm{nphGdem}\ ^-]$	8.43×10^{1}	2.0×10^{7}	30[b]
17	$\mathrm{nphG}\alpha\beta O(f) + 1G(-f) \rightarrow \mathrm{nphG}\alpha\beta O(aq) + 1G(-aq)$	$[\mathrm{nphG}\alpha\beta O][G^-]$	3.32	1.0×10^{5}	25[b]
18	$\alpha\mathrm{COnphG}\beta\gamma S(f) + 1.7G(-f) \rightarrow \alpha\mathrm{COnphG}\beta\gamma S(aq) + 1.7G(-aq)$	$[\alpha\mathrm{COnphG}\beta\gamma S][G^-]$	1.62×10^{3}	1.0×10^{5}	10[b]
19	$\alpha\mathrm{COnphG}\beta\gamma S(f) + 1.8\alpha\beta\mathrm{conj}G(-f)$ $\rightarrow \alpha\mathrm{COnphG}\beta\gamma S(aq) + 1.8\alpha\beta\mathrm{conj}G(-aq)$	$[\alpha\mathrm{COnphG}\beta\gamma S][\alpha\beta\mathrm{conj}G\ ^-]$	3.23×10^{3}	2.0×10^{5}	10[b]
20	$\alpha\mathrm{COnphG}\beta\gamma S(f) + 2\mathrm{Cat}(-f) \rightarrow \alpha\mathrm{COnphG}\beta\gamma S(aq) + 2\mathrm{Cat}(-aq)$	$[\alpha\mathrm{COnphG}\beta\gamma S][\mathrm{Cat}^-]$	4.11×10^{2}	2.0×10^{5}	15[b]
21	$\alpha\mathrm{COnphG}\beta\gamma S(f) + 2\mathrm{nphGdem}(-f)$ $\rightarrow \alpha\mathrm{COnphG}\beta\gamma S(aq) + 2\mathrm{nphGdem}(-aq)$	$[\alpha\mathrm{COnphG}\beta\gamma S][\mathrm{nphGdem}\ ^-]$	6.46×10^{3}	4.0×10^{5}	10[b]
22	$\alpha\mathrm{COnphG}\beta\gamma S(f) + 1G(-f) \rightarrow \alpha\mathrm{COnphG}\beta\gamma S(aq) + 1G(-aq)$	$[\alpha\mathrm{COnphG}\beta\gamma S][G^-]$	3.32	1.0×10^{5}	25[b]

[a] Kinetic parameters were obtained from regression in Kinfit software, experimental values were obtained from published studies.[45−48] [b] Kinetic parameters were obtained from regression in Kinfit software; experimental values were obtained from published studies.[20,32,50]

reaction involving the cleavage of the β-ether bonds by epoxide formation **S14** (G$\alpha\beta$O$^-$) and guaiacol **S1** (G) liberation may take place, especially at high alkalinity[3] (Table 3, reaction 3).

Reactions of Non-Phenolic Lignin Units. Alkaline cleavage of the β-*O*-4 linkage in a non-phenolic structure proceeds through the participation of an ionized α- or γ-hydroxyl group.[36] As shown in Figure 1b, the reaction leads to the formation of an oxirane **S11** (nphG$\alpha\beta$O), which then reacts further to **S12** (nphGβNu) depending on the nucleophiles present. This is the most important lignin degradation reaction that takes place in the bulk delignification phase. Two studies, conducted by Miksche[36] and Gierer,[34] were taken into account. Parameters were fitted in Kinfit[33] software, in order to obtain the kinetic parameters presented in Table 3 (reaction 6). Nucleophiles, such as HS$^-$ and HO$^-$, can attack and open the formed oxirane structure. This reaction promotes efficient delignification by fragmenting the lignin and by generating new free phenolic hydroxyl groups, which play a crucial role in the overall delignification process.[1,40] In cases where nucleophilic sites in lignin or carbohydrates are present, the reaction will result in condensation products.[1]

The non-phenolic lignin units are difficult to degrade; however, the alkaline cleavage of β-ether bonds in non-phenolic units can be facilitated by the presence of α- or γ-carbonyl functionality.[41] The cleavage of β-*O*-4 bonds in non-phenolic units with α-carbonyl functionality takes place under ambient conditions.[42] The reaction mechanism is presented in Figure 1c. First, structure **S2** (αCOnphG) reacts with HO$^-$ and forms structure **S9** (αCOnphG$\beta\gamma$conj) which further reacts with HS$^-$, forming **S10** (αCOnphG$\beta\gamma$S) as a result of the cleavage of the β-ether bond. The kinetic parameters for **S9** formation were published by Miksche[43] and Gierer.[41] Recently we conducted additional experimental work[42] in order to obtain kinetic parameters for the second step and more precise data on the first step of the reaction (Table 3, reactions 4 and 5, respectively).

Demethylation Reactions. Non-phenolic lignin units also undergo demethylation by hydrogen sulfide and methyl mercaptide ions, forming methyl mercaptan and dimethyl sulfide, respectively (Figure 1, reaction d).[44−48] The kinetic parameters for the demethylation reaction by hydrogen sulfide and methyl mercaptide ions were obtained by fitting kinetic parameters against experimental data presented in the literature[45,47,48] (Table 3, reactions 7−11).

Modeling of Lignin Dissolution. After modeling the lignin fragmentation reactions, the macromolecular nature of lignin was taken into account in the modeling of lignin dissolution. When describing the conditions for lignin dissolution, it was assumed that the rate of dissolution correlates with (i) the cleavage of β-aryl ether bonds in non-phenolic lignin units and (ii) liberation of new ionized phenolic units. Previously, Tarvo et al.[49] applied a similar lignin dissolution scheme for modeling the chlorine dioxide delignification stage. In that model, the lignin units promoting the dissolution were lignin's acidic reaction products (muconic acid, etc.).

The applied lignin dissolution schemes and rate equations are summarized in Table 3 (reactions 12−21). The dissolution stoichiometry and the kinetic parameters were fitted using Kinfit software using data from wood meal pulping studies.[20,30,32] The low activation energy values (10−30 kJ mol^{-1}) indicate that the dissolution was modeled to be fast in comparison with the slower degradation reactions. It should also be noted that the applied schemes provide a mathematical solution to explain the experimental data rather describe truly the complex dissolution phenomena.

Model Validation. The comparison between experimental and modeling results regarding lignin structures could not be done on a molecular scale, because reliable analytical data for detailed characterization of the residual and dissolved lignin were not available. Consequently, the simulation results were converted into standardized variables such as kappa number and lignin yield, in order to make the evaluation. Tarvo et al.[49] presented a detailed explanation of the kappa number and lignin yield calculations in Flowbat software. The lignin content (weight percent) is calculated as presented in eq 1. The kappa number is computed by taking into account only compounds bound to the solid fiber wall. Equation 2 is utilized to convert the content of unsaturated structures in pulp into the kappa number. The compound-specific oxidation equivalent values utilized in the model are listed in Table 4.

$$L = 100\% \sum_i \left(\frac{\mathrm{OxEq}_i}{\mathrm{OxEq}_{\mathrm{arom}}} M_{\mathrm{w},i} c_i \right) / 1000 \tag{1}$$

$$\mathrm{kappa} = \frac{\sum_i (\mathrm{OxEq}_i M_{\mathrm{w},i} c_i)}{0.10} \tag{2}$$

Table 4. Oxidation Equivalent Values Assigned for the Lignin

pseudocompound	assigned oxid equiv value
full aromatic ring[a]	16
quinone	10
muconic acid	12
maleic acid	11

[a] Phenolic and non-phenolic lignin compounds.

where L = lignin content (wt %), $M_{\mathrm{w},i}$ = molar weight of component i (g/mol), c_i = component concentration (mol/kg fiber), OxEq_i = oxidation equivalent value of component i, and $\mathrm{OxEq}_{\mathrm{arom}}$ = oxidation equivalent value of full aromatic ring.

RESULTS AND DISCUSSION

For the delignification model development, experimental work from the study by Bogren et al.[20,50] was utilized. Since their original experimental data was not reported in the paper, the experimental data points were generated with Matlab software by using their reported model.[20,51] Further in the text, these reproduced experimental data points will be called "experimental results" and used for validation of our model. Additionally, original experimental results from Paananen et al.[30−32] were used for the model validation and development. Both Bogren et al.[20,50] and Paananen et al.[30−32] used wood meal (particle size <1 mm) and a high liquor-to-wood ratio (200:1) to eliminate the effects of mass transfer and time-dependent changes in the hydroxyl ion concentrations on the results.

Figures 2−6 compare simulation results from our delignification model with Bogren's[20,51] experimental data. In the first set of experiments, represented by Figures 2−4, the hydroxyl ion concentration was kept constant at 0.26 M while the concentration of HS$^-$ ion was varied from 0.1 to 0.52 M. In general, the phenomenon-based model predicted well the dependence of the degree of delignification on temperature, time, and HS$^-$ ion concentration. However, at the lowest (0.1

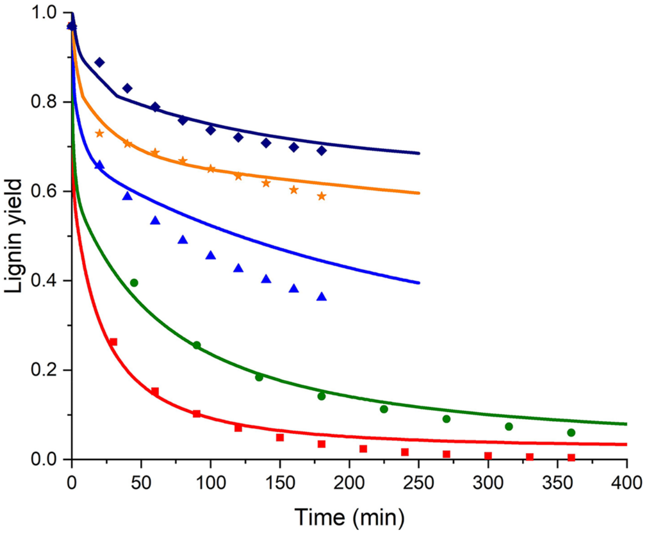

Figure 2. Delignification of pine wood meal: simulation (lines) and experimental results[51] (symbols). Experimental and simulation conditions: $[HO^-]$ = 0.26 M, $[HS^-]$ = 0.52 M (■, 168 °C; ●, 154 °C; ▲, 139 °C; ★, 123 °C; ◆, 108 °C).

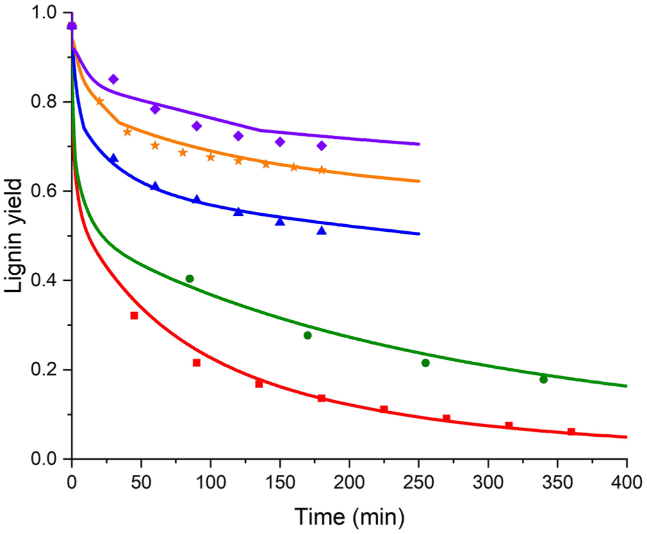

Figure 3. Delignification of pine wood meal: simulation (lines) and experimental results[51] (symbols). Experimental and simulation conditions: $[HO^-]$ = 0.26 M, $[HS^-]$ = 0.26 M (■, 168 °C; ●, 154 °C; ▲, 139 °C; ★, 123 °C; ◆, 108 °C).

M) HS^- ion concentration, the model overestimated the rate of delignification at higher temperatures (≥139 °C) (Figure 4). One of the functions of the HS^- ion in kraft pulping is to prevent condensation of lignin fragments by blocking their reactive sites, such as the benzylic carbon.[27] However, these lignin condensation reactions were not included in the delignification model, which could be the reason for the overestimation of the delignification rate at low HS^- concentration.

Our model was targeted to be an exceptional tool for detailed modeling; consequently, it is very important to see the influence of the hydroxide ion concentration on the delignification process, in the case of constant hydrogen sulfide ion concentration. Correlation between the model prediction and the experimental results are good as presented in Figures 5 and 6.

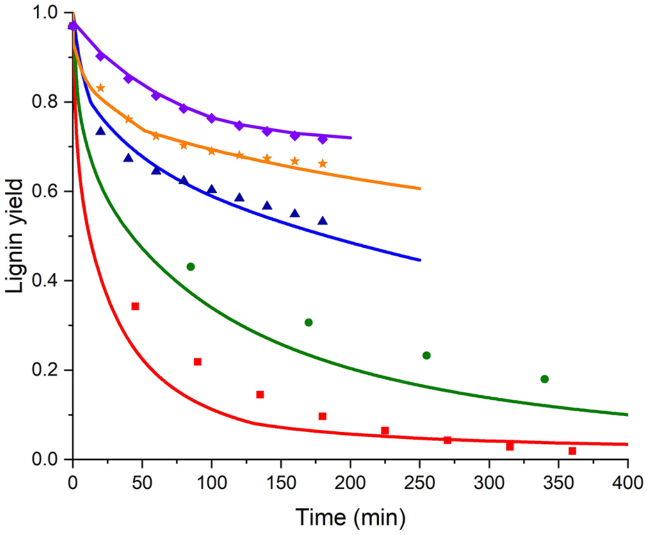

Figure 4. Delignification of pine wood meal: simulation (lines) and experimental results[51] (symbols). Conditions: $[HO^-]$ = 0.25 M, $[HS^-]$ = 0.10 M (■, 168 °C; ●, 154 °C; ▲, 139 °C; ★, 123 °C; ◆, 108 °C).

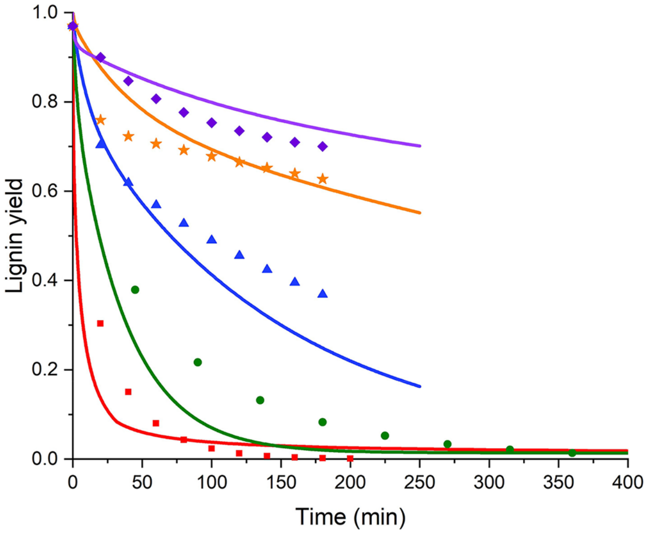

Figure 5. Delignification of pine wood meal: simulation (lines) and experimental results[51] (symbols). Conditions: $[HO^-]$ = 0.78 M, $[HS^-]$ = 0.26 M (■, 168 °C; ●, 154 °C; ▲, 139 °C; ★, 123 °C; ◆, 108 °C).

In the second set of experiments, the hydroxyl ion concentration was varied from 0.1 to 0.78 M while the concentration of the HS^- ion was kept constant at 0.26 M (Figures 3, 5, and 6). In general, the model predicted the time dependence of delignification properly at the applied temperature and hydroxyl ion concentration levels. The only clear exception seemed to the combination of the highest hydroxyl ion concentration (0.75 M) with the highest temperature (168 °C) where the model produced significantly faster delignification than what was experimentally observed (Figure 5). On the other hand, a similar discrepancy was also seen with the experimental data of Paananen et al.,[30,32] who studied the delignification at 1.55 M hydroxyl ion concentration (Figure 7). In fact, the simulation reproduced the data of Paananen et al.[30] very well, suggesting that the modeling principles were well justified. In all, taking into account the complexity of

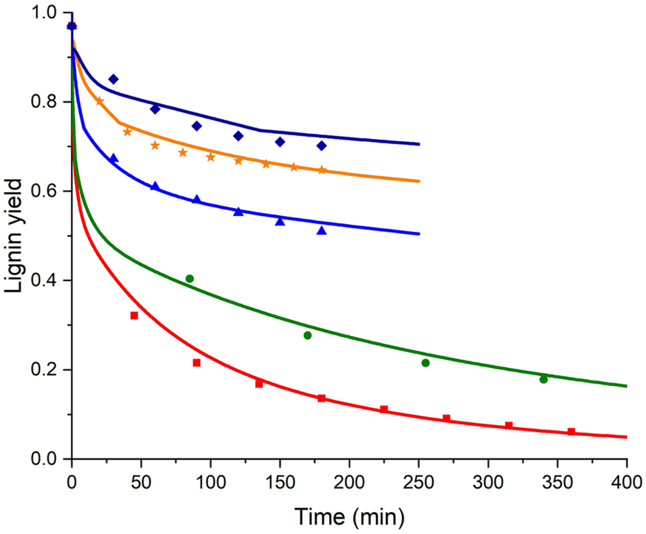

Figure 6. Delignification of pine wood meal: simulation (lines) and experimental results[51] (symbols). Conditions: $[HO^-] = 0.1$ M, $[HS^-] = 0.25$ M (■, 168 °C; ●, 154 °C; ▲, 139 °C; ★, 123 °C; ◆, 108 °C).

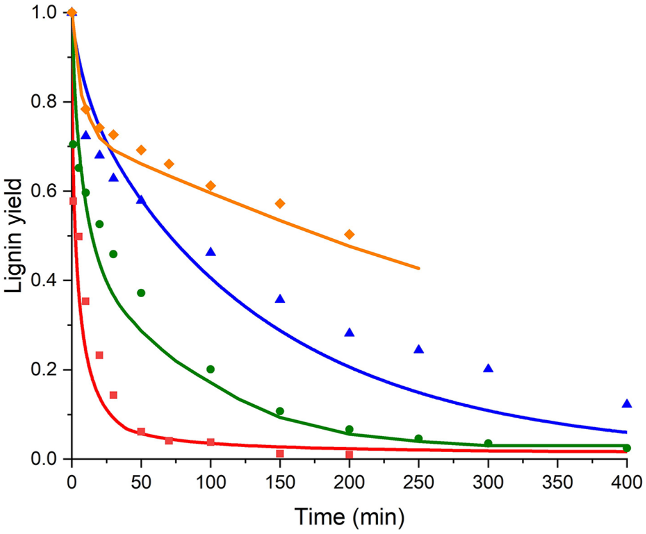

Figure 7. Delignification of pine wood meal: simulation (lines) and experimental results[30] (symbols). Conditions: $[HO^-] = 1.55$ M, $[HS^-] = 0.31$ M (■, 160 °C; ●, 150 °C; ▲, 140 °C; ◆, 130 °C).

delignification and amount of input data in the model, the correlation with experimental results was good.

Initial, bulk, and residual stages of delignification are visible in Figures 2−7. The main lignin reactions occur during the first two phases: initial and bulk. In the initial phase, delignification proceeds mainly due to the reaction of phenolic and carbonyl structures. As result, around 20% of lignin degrades in the initial phase. The main part of lignin is removed in the bulk phase. In the residual phase a very small amount of lignin is dissolved. The main reasons for the retarded delignification in the residual phase are reported to be the presence of alkaline-stable native lignin structure, the presence of alkaline-stable covalent linkages between lignin and carbohydrates, and the condensation reactions occurring in lignin.[56] Although the model simulated well the initial and bulk delignification stages, it often underestimated the importance of the residual delignification stage. Even though we aimed at modeling the delignification real chemical reactions, we did not include all possible degradation and condensation reactions of lignin and the conditions for its solubilization. While the residual lignin may still contain significant amounts of degradable *β*-*O*-4 ether bonds, chemical bonding to the cell wall polysaccharides and stable interunit linkages formed through condensation reactions may prevent lignin from solubilizing. Other features that we did not include in the model include, e.g., aryl group migration reactions and stereochemical and thermodynamic aspects of lignin degradation and dissolution.[52]

Because the model is based on real chemical reactions, it is flexible in monitoring the contents of various chemical structures and technical parameters. In Figure 8, simulated kappa numbers are compared with experimental data points from Paananen et al.[53] The fitting was good, and predicted results were close to the experimental data. Other engineering parameters that could be computed from the detailed chemical composition of the reaction system include, e.g., intrinsic viscosity, brightness, and yield of the pulp, as well as active alkali, effective alkali, sulfidity, and the higher heating value of the black liquor.

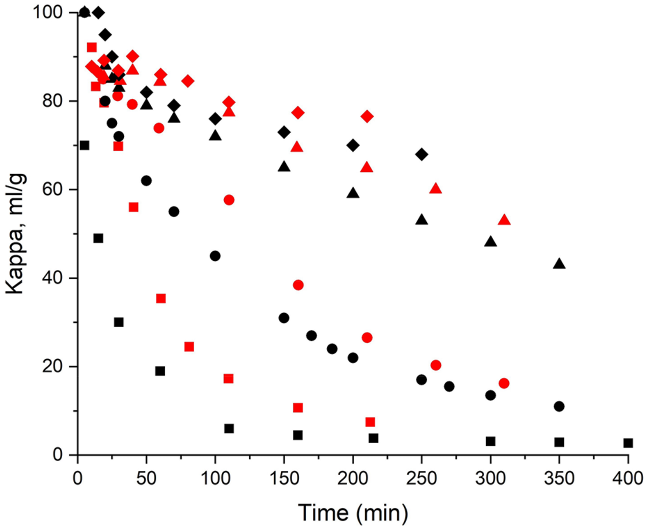

Figure 8. Simulation (black symbols) and experimental results (red symbols) of kappa number at $[HO^-] = 1.55$ M and $[HS^-] = 0.31$ M (■, 160 °C; ●, 150 °C; ▲, 140 °C; ◆, 130 °C).

Certain reactions, as mentioned earlier, are missing from the model, and inclusion of those could improve the model further. Yet another aspect, which could either promote or prevent lignin dissolution, is the presence of lignin−carbohydrate linkages.[53] Part of the work related to carbohydrate chemistry is presented in another article.[55] Lignin−carbohydrate linkages are not taken into consideration in the current work. Besides lignin fragmentation and ionization, lignin dissolution is also dependent on ionic strength, alkalinity, and dissolved wood components in black liquor. Increase in ionic strength during cooking leads to increased delignification rate with increasing pulp yield. Additionally, dissolved wood components promote the delignification and increase in yield. It is known that phenolic lignin units promote dissolution; however, it is also possible that saccharine acid could increase lignin dissolution.[57] The model could be improved by introduction of certain physicochemical aspects of lignin reactivity. For example, lignin reactions in the fiber wall (immobilized components) should have different kinetic parameters from lignin reactions in the liquid phase (dissolved components). In the model, we assumed that the kinetic parameters are the same in both phases (fiber/solid and external/liquid). In the present model, experimental studies from lignin model compounds (dimer cleavage) have been utilized; however, reactions in macromolecules may occur differently. Obst[54] has claimed that kraft delignification of wood cannot be described by simple lignin models because in reality the delignification process is more complex. Moreover, the current hypothesis about lignin dissolution could be somewhat inaccurate. It is possible that lignin dissolution should be modeled based on solubility rather than on chemical reactions. Lignin is a polymer, and the movement of large polymer molecules is spatially restricted. That is why chemical degradation is important. Besides the chemical structure, the physical state of a polymer is also important for its solubility properties. Studies[36,52,54] have shown the effect of *erythro* and *threo* isomers of *β*-*O*-4 structures on lignin degradation and dissolution. The activation energy of the *threo* isomer was reported to be always higher than that of its *erythro* counterpart for all phases of delignification.[52] Based on the description above, it would be beneficial to take into account thermodynamics in the delignification process. However, already at this point, simulation results give a reasonable fitting and good correlation with the experimental data.

■ CONCLUSIONS

This paper introduces a detailed model for delignification in kraft pulping, extending earlier work for chemical pulp bleaching and hot water extraction. In this part, lignin fragmentation and dissolution of the fragments were considered. As result of this work, it is possible to fit the model to experimental data very well at different temperatures and chemical compositions of the cooking liquor. However, our hypothesis on lignin dissolution may require additional improvements. At present, the model is able to predict the chemical composition of the fiber wall, as well as the black liquor composition with good correlation. Moreover, such engineering parameters as the kappa number, effective alkali, active alkali, sulfidity, total alkali, and higher heating value can be computed from the detailed chemical composition of the liquor and wood or chemical pulp.

■ AUTHOR INFORMATION

Corresponding Author

Olesya Fearon − *Department of Bioproducts and Biosystems, School of Chemical Engineering, Aalto University, FI-00076 Aalto, Finland;* orcid.org/0000-0003-0826-0475; Email: olesya.fearon@aalto.fi

Authors

Susanna Kuitunen − *Neste Jacobs Oy, FI-06101 Porvoo, Finland*

Kyösti Ruuttunen − *Department of Bioproducts and Biosystems, School of Chemical Engineering, Aalto University, FI-00076 Aalto, Finland*

Ville Alopaeus − *Department of Chemical and Metallurgical Engineering, School of Chemical Engineering, Aalto University, FI-00076 Aalto, Finland*

Tapani Vuorinen − *Department of Bioproducts and Biosystems, School of Chemical Engineering, Aalto University, FI-00076 Aalto, Finland;* orcid.org/0000-0002-5865-1776

Complete contact information is available at: https://pubs.acs.org/10.1021/acs.iecr.0c02110

Notes

The authors declare no competing financial interest.

■ ACKNOWLEDGMENTS

Financial support from FIBIC (EffFibre Research Program) is gratefully acknowledged. The authors would like to thank Markus Paananen for kindly providing us the experimental data.

■ NOTATION

A = frequency factor (depends on rate equation)
E_a = activation energy (J mol^{-1})
EF = effective alkali
FSP = fiber saturation point (kg of water (kg of oven dried wood)$^{-1}$)
k = reaction rate constant (stoichiometry dependent units)
K = equilibrium constant (stoichiometry dependent units)
L:W = liquid-to-wood ratio
t = time (s)
T = temperature (K)

■ REFERENCES

(1) Sjöström, E. *Textbook of Wood Chemistry: Fundamentals and Applications*, 2nd ed.; Academic Press Inc.: San Diego. 1993.

(2) Adler, E. Lignin chemistry -past, present and future. *Wood Sci. Technol.* **1977**, *11*, 169−218.

(3) Gierer, J.; Ljunggren, S. The reaction of lignins during sulfate pulping part 16. The kinetic cleavage of the betta-aryl ether linkages in structures containing carbonyl groups. *Sven. Papperstidn.* **1979**, 3, 71.

(4) Kerr, A. The kinetic of kraft pulping - batch digester control. *Tappi* **1976**, *59* (5), 89−91.

(5) Cherubini, F. The biorefinery concept: Using biomass instead of oil for producing energy and chemicals. *Energy Convers. Manage.* **2010**, *51*, 1412−1421.

(6) Demuner, I. F.; Colodette, J. L.; Demuner, A. J.; Jardim, C. M. Biorefinery review: Wide-reaching products through kraft lignin. *BioResources.* **2019**, *14* (3), 7543.

(7) Ooi, Z.; Harruddin, N.; Othman, N. Recovery of kraft lignin from pulping wastewater via emulssion liquid membrane process. *AIChE J.* **2015**, *31* (5), 1305−1314.

(8) Zhang, Y.; Yuan, Z.; Xu, C. Engineering biomass into formaldehyde-free phenolic resin for composite materials. *AIChE J.* **2015**, *61* (4), 1275−1283.

(9) Yuan, T.; Xu, F.; Sun, R. Role of lignin in a biorefinery: Separation characterization and valorization. *J. Chem. Technol. Biotechnol.* **2013**, *88*, 346−352.

(10) Vroom, K. E. The H-factor: A means of expressing cooking times and temperatures as a single variable. *Pulp Paper Mag. Can.* **1957**, *58*, 228−231.

(11) Hatton, J. V. Development of yield prediction equations in kraft pulping. *Tappi J.* **1973**, *56*, 97.

(12) Clayton, D.; Easty, D.; Einsparhr, D.Chapter IV. Kinetics and Modeling of Kraft Pulping. *Alkaline Pulping*; Pulp and Paper Manufacture 5; Join Textbook Committee of the Paper Industry: 1989; pp 45−73.

(13) Smith, C. C.; Williams, T. J. *Mathematical Modeling, Simulation and Control of the Operation of a Kamyr Continuous Digester for the Kraft Process.* Ph.D. Thesis, Purdue University, West Lafayette, IN, 1974.

(14) Kleinert, T. N. Mechanism of alkaline delignification. I. the overall reaction patern. *Tappi J.* **1966**, *49* (2), 53−57.

(15) Saltin, J. F. A predictive dynamic model for continuous digester. *Predictive Dynamic Model for Continuous Digesters. 1992 Pulping Conference Proceedings*; TAPPI: 1992; p 261.

(16) Burazin, M. A.; McDonough, T. J. Building a mechanistic model of kraft-anraquinone pulping kinetics. *IPC Technical Paper Series* **1987**, No. 250, 1−7.

(17) Gustafson, R. R.; Sleicher, C. A.; McKean, W. T.; Finlayson, B. A. Theoretical model of the kraft pulping process. *Ind. Eng. Chem. Process Des. Dev.* **1983**, *22* (1), 87−96.

(18) LeMon, S.; Teder, A. Kinetics of the delignification in kraft pulping. *Sven. Papperstidn.* **1973**, *76* (11), 228.

(19) Nieminen, K.; Kuitunen, S.; Paananen, M.; Sixta, H. Novel insight into lignin degradation during kraft cooking. *Ind. Eng. Chem. Res.* **2014**, *53*, 2614−2624.

(20) Bogren, J.; Brelid, H.; Theliander, H. Towards a general kraft delignification model. *Nord. Pulp Pap. Res. J.* **2009**, *24* (1), 33−37.

(21) Choi, H.; Kwon, J. S. Multiscale modeling and control of kappa number and porosity in a batch pulp digester. *AIChE J.* **2019**, *65* (6), No. e16589.

(22) Choi, H.; Kwon, J. S. Modeling and control of cell wall thickness in batch delignification. *Comput. Chem. Eng.* **2019**, *128*, 512−523.

(23) Treimanis, A.; Maloney, T.; Klevinska, V.; Eisimonte, M.; Paulapuro, H. The swelling behavior of spruce wood cell walls during kraft pulping. *Lenzinger Berichte* **2000**, *79*, 137−142.

(24) Lehto, J. H. Characterization of mechanical and chemical pulp fibers. *58th Appita Annual Conference and Exhibition, Canberra, ACT, Australia, April 19−21, 2014*; Appita: 2004; Paper 3A13, 8.

(25) Kuitunen, S. *Phase and Reaction Equilibria in the Modelling of Hot Water Extraction, Pulping and Bleaching*. Ph.D. Thesis, Aalto University, 2014.

(26) Kuitunen, S.; Vuorinen, T.; Alopaeus, V. The role of donnan effect in kraft liquour impregnation and hot water extraction. *Holzforschung* **2013**, *67*, 511−521.

(27) Santos, R. B.; Hart, P.; Jameel, H.; Chang, H. Wood based lignin reactions important to the biorefinery and pulp and paper industries. *BioResources* **2012**, *8* (1), 1456−1477.

(28) Tarvo, V.; Kuitunen, S.; Aittamaa, J. Advanced approach on modelling chemical pulp bleaching. *PulPaper 2007 Conference: Innovative and Sustainable use of Forest Resources*; Finnish Paper Engineers' Association: 2007.

(29) Kuitunen, S.; Tarvo, V.; Rovio, S.; Liitiä, T.; Vuorinen, T.; Alopaeus, V. Modeling of alkaline extraction chemistry and kinetics of softwood kraft pulp. *Holzforschung* **2014**, *68*, 733−746.

(30) Paananen, M.; Liitiä, T.; Sixta, H. Further insight into carbohydrate degradation and dissolution behavior during kraft cooking under elevated alkalinity without and in the presence of anthraquinone. *Ind. Eng. Chem. Res.* **2013**, *52*, 12777−12784.

(31) Paananen, M.; Tamminen, T.; Nieminen, K.; Sixta, H. Galactoglucomannan stabilization during the initial kraft cooking of scots pine. *Holzforschung* **2010**, *64* (6), 683−692.

(32) Paananen, M.; Rovio, S.; Liitiä, T.; Sixta, H. Effect of hydroxide and sulfite ion concentration in alkaline sulfite anthraquinone (ASA) pulping − a comparative study. *Holzforschung* **2015**, *69* (6), 661−666.

(33) Kuitunen, S. *KINFIT Manual Tailored for VIP/VIC Models Users*; Aalto University: June 2011; pp 2−11.

(34) Gierer, J.; Ljunggren, S. The reactions of lignin during sulfate pulping part 17. kinetic treatment of the formation and competing reactions of quinone methide intermediates. *Sven. Papperstidn.* **1979**, *17*, 502.

(35) Kondo, R.; Tsutsumi, Y.; Imamura, H. Kinetics of beta-aryl ether cleavage of phenolic syringyl type lignin model compounds in soda and kraft systems. *Holzforschung* **1987**, *41*, 83−88.

(36) Miksche, G. E. Zum alkalischen abbau der p-alkoxy-arylglycerin-beta-arylätherstrukturen des lignins. Versuche mit erythro-veratrylglycerin-beta-guajacyläther. *Acta Chem. Scand.* **1972**, *26*, 3275.

(37) Gierer, J. Chemical aspects of kraft pulping. *Wood Sci. Technol.* **1980**, *14* (4), 241−266.

(38) Dimmel, D.; Gellerstedt, G. Chemistry of alkaline pulping. In *Lignin and Lignans: Advances in Chemistry*; Heitner, C., Dimmel, D., Schmidt, J., Eds.; CRC Press, Taylor & Francis.: Boca Raton, FL; 2010; pp 349−393.

(39) Gellerstedt, G. Pulping chemistry. In *Wood and Cellulosic Chemistry*, 2nd ed.; Hon, D. N., Shiraishi, N., Eds.; Marcel Dekker, Inc.: 2001; pp 859−986.

(40) Dimmel, D. R.; Schuller, L. F. Structural/reactivity studies (I): Soda reactions of lignin model compounds. *J. Wood Chem. Technol.* **1986**, *6* (4), 535−552.

(41) Gierer, J.; Ljunggren, S. The reactions of lignin during sulfate pulping part 18. the significance of alpha-carbonyl groups for the cleavage of betta-aryl ether structures. *Sven. Papperstidn.* **1980**, *3*, 75.

(42) Fearon, O.; Kuitunen, S.; Vuorinen, T. Reactions of strong nucleophiles with non-phenolic lignin units with α-carbonyl functionality in aqueous alkali. *Holzforschung* **2016**, *70* (9), 811−818.

(43) Miksche, G. E. Lignin Reactions in Alkaline Pulping Processes (Rate processes in Soda Pulping). *Chemistry of Delignification with Oxygen, Ozone and Peroxides. 1st International Symposium*; 1975; p 107.

(44) Douglass, I.; Price, L. A study of methyl mercaptan and dimethyl sulfide formation in kraft pulping. *Tappi J.* **1966**, *49* (8), 335−342.

(45) Turunen, J. *Demethylation and Degradation of Simple Lignin Model Compounds by Pressure Digestion with Aqueous Sodium Hydrogen Sulfide, Sodium Methyl Mercaptide and Sodium Hydroxide Solutions*. Ph.D. Thesis. University of Helsinki, Helsinki, 1963.

(46) McKean, W. T., Jr.; Hrutfiord, B. J.; Sarkanen, K. V.; Price, L.; Douglass, I. B. Effect of kraft pulping conditions on the formation of methyl mercaptan and dimethyl sulfate. *Tappi J.* **1967**, *50* (8), 400−405.

(47) McKean, W. T., Jr.; Hrutfiord, B. F.; Sarkanen, K. V. Kinetic analysis of odor formation in the kraft pulping process. *Tappi J.* **1965**, *48* (12), 699−704.

(48) McKean, W. T., Jr.; Hrutfiord, B. F.; Sarkanen, K. V. Kinetics of methyl mercaptan and dimethyl sulfide formation in kraft pulping. *Tappi J.* **1968**, *51* (12), 564−567.

(49) Tarvo, V.; Lehtimaa, T.; Kuitunen, S.; Alopaeus, V.; Vuorinen, T.; Aittamaa, J. A model for chlorine dioxide delignification of chemical pulp. *J. Wood Chem. Technol.* **2010**, *30* (3), 230−268.

(50) Bogren, J.; Brelid, H.; Theliander, H. Reactions kinetics of softwood kraft delignification - general considerations and experimental data. *Nord. Pulp Pap. Res. J.* **2007**, *22* (2), 177−183.

(51) Bogren, J.; Brelid, H.; Theliander, H. Assessment of reaction kinetic models describing delignification fitted to well-defined kraft cooking data. *Nord. Pulp Pap. Res. J.* **2008**, *23* (2), 210−217.

(52) Ahvazi, B. C.; Argyropoulos, D. S. Thermodynamic parameters governing the steroselective degradation of arylglycerol-B-aryl ether bonds in milled wood lignin under kraft pulping conditions. *Nord. Pulp Pap. Res. J.* **1997**, *12*, 282−288.

(53) Jääskeläinen, A.; Willberg Keyriläinen, P.; Liitiä, T.; Tamminen, T. Carbohydrate-free and highly soluble softwood kraft lignin fractions by aqueous acetone evaporation fractionation. *Nord. Pulp Pap. Res. J.* **2017**, *32* (4), 485−492.

(54) Obst, J. R. Kinetic of alkaline cleavage of B-aryl ether bonds in lignin models: significance to delignification. *Holzforschung* **1983**, *37* (1), 23−28.

(55) Fearon, O.; Nykänen, V.; Kuitunen, S.; Ruuttunen, K.; Alén, R.; Alopaeus, V.; Vuorinen, T. Detailed modeling of kraft pulping chemistry: Carbohydrate Reactions. *AIChE J.* **2020**, No. e16252.

(56) Lawoko, M. *Lignin Polysaccharide Network in Softwood and Chemical Pulps: Characterisation, Structure and Reactivity*. Ph.D. Thesis, Royal Institute of Technology, 2005.

(57) Sjödahl, R. G.; Ek, M.; Lindström, M. E. The effect of sodium ion concentration and dissolved wood components on the kraft pulping of softwood. *Nord. Pulp Pap. Res. J.* **2004**, *19* (3), 325−329.